Ab initio study of the one-dimensional H-bonded ferroelectric CsH_2PO_4

J. Lasave, P. Abufager, and S. Koval
Instituto de Física Rosario, CONICET and Universidad Nacional de Rosario, 27 de Febrero 210 Bis, 2000 Rosario, Argentina
(Received 29 August 2015; revised manuscript received 29 December 2015; published 20 April 2016)

We studied the microscopic mechanism of the paraelectric-ferroelectric (PE-FE) phase transition of CsH_2PO_4 (CDP) by means of first-principles electronic structure calculations. The calculated structural parameters in the PE and FE phases as well as the total spontaneous polarization P_s obtained with the Berry phase formalism for CDP are in good agreement with experiments. The main contribution to P_s originates from a large yx component of the calculated Born effective-charge tensor for the disordered protons. Moreover, this component is ≈2.7 times larger than the zx component of the proton effective-charge tensor relevant to the polarization in the H-bonded FE KH_2PO_4 (KDP). This is the main feature that compensates the different number of protons per formula unit involved in the phase transitions for CDP and KDP to give close values for their measured P_s. Correlations among protons and heavy atoms along chains in the b direction lead to larger instabilities for the global and local FE distortions in CDP and its deuterated counterpart DCDP. We conclude that the tunneling particle is a dressed proton (deuteron) in agreement with experiments and with recent *ab initio* results for KDP.

DOI: 10.1103/PhysRevB.93.134112

I. INTRODUCTION

Cesium dihydrogen phosphate (CsH_2PO_4, or CDP) is a solid acid compound that belongs to a large family of H-bonded ferroelectrics whose prominent member is KH_2PO_4 (KDP) [1]. CDP shows good conductivity at high temperature and low-temperature ferroelectric (FE) properties. It undergoes a superprotonic transition showing an increase by three orders of magnitude in the proton conductivity above 503 K [2,3]. Due to this behavior, there was a renewed interest in CDP as a viable electrolyte for intermediate temperature (470–570 K) fuel cells [4,5]. CDP is also interesting from a fundamental point of view. It displays a quasi-1D FE phase transition at atmospheric pressure, which differs from the 3D nature of the FE ordering observed in KDP [1]. Also intriguing is the fact that the FE phase of CDP transforms to different AFE phases by applying increasing pressure at low temperature [6,7]. The paraelectric-ferroelectric (PE-FE) phase transition in CDP arises at a critical temperature $T_c \approx 150$ K, which is close to the corresponding value for KDP (≈122 K). There is a huge isotope effect in the PE-FE transition of CDP with a T_c increase of ≈110 K for the deuterated compound CsD_2PO_4 (DCDP) [8], which is remarkably similar to the corresponding increase produced by deuterating KDP. This giant isotope effect is a common feature in the whole family of H-bonded FE materials and its origin still remains unclear. Particularly, the connection between the isotope effect, the Ubbelohde (or geometrical) effect [9,10] and the proton tunneling [11,12] is not yet well understood. Recent theoretical works attempted to explain the link between tunneling and geometrical effects in KDP and squaric acid [13–17]. However, a detailed knowledge about the PE-FE phase transition of CDP and related compounds is still lacking. It is intriguing in particular that the measured values for the saturated polarization P_s in CDP and KDP, 5.3 and 5.1 $\mu C/cm^2$, respectively, and the effect of deuteration on P_s are very similar in both compounds despite the different dimensionality and the different number of protons per formula unit involved in their FE transitions [18,19]. In this work, we perform confident *ab initio* calculations based on density functional theory with the purpose of shedding light on the microscopic mechanism of the PE-FE phase transition of CDP.

The crystal structure of the PE phase of CDP is monoclinic ($P2_1m$) at room temperature with two formula units (f.u.), as depicted in Fig. 1(a). The phosphates in this structure are linked by two types of H bonds, namely, short and long. The short H bonds connect the phosphates forming a chain that runs along the b axis. Following similar notation from Ref. [20], for these short H bonds we label the hydrogens H_2 and the corresponding oxygens O_3 and O_4 [see Fig. 1(a)]. The H_2's are disordered over two equivalent sites along the H bonds in the PE phase. They become ordered at T_c as they move along the pattern of the FE mode as shown in Fig. 1(a). With these mode distortions, the crystal transforms to $P2_1$ symmetry and the FE phase arises. The origin of the PE-FE transition is ascribed to the H_2's ordering in the chains running along the b direction and the transition is considered to have a one-dimensional character. The chains formed by the short H bonds O_3-H_2-O_4 are linked in a transverse direction by longer H bonds where the H's are always ordered at any temperature and do not contribute to the FE ordering [21]. The hydrogens of the long H bond are labeled H_1 and the corresponding oxygens O_1 and O_2, in correspondence to the notation used in Ref. [20] [see Fig. 1(a)].

The quasi-one-dimensional character of the PE-FE transition in CDP is revealed by different experiments. Neutron-scattering experiments show that strong correlations along the H-disordered chains in the b direction arises near the critical temperature in the PE phase of DCDP [22]. In this study, it is roughly estimated at $T = 267$ K a correlation length of ≈250 Å along the chains, which falls to ≈100 Å (≈15 unit cells) at room temperature. Deviations from the Curie-Weiss law found in dielectric measurements are also in accordance with the quasi-1D nature of the transition [18,23].

From the theoretical side, a common approach was to use the quasi-1D Ising model with intrachain and interchain couplings between pseudospins, including also the interaction with the external electric field [18,23–26]. The interchain interaction is much smaller than the intrachain counterpart, and is treated by means of a mean-field theory. This model accounts well for the static dielectric constant data except in the vicinity of T_c, where three dimensional correlations, possibly arising from interchain electrostatic dipolar interactions, could be also

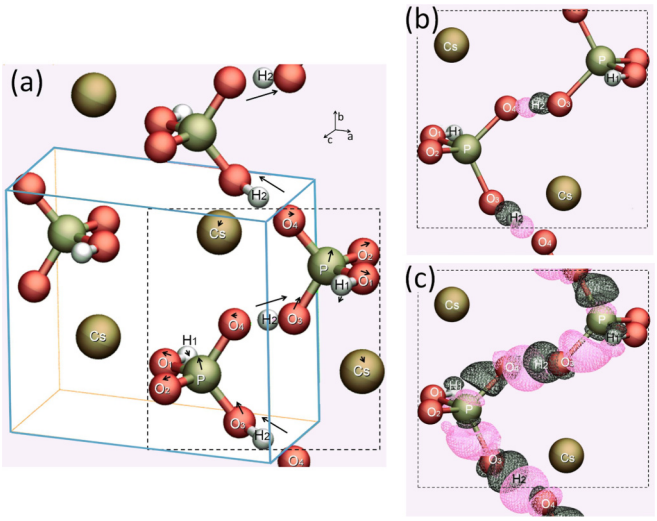

FIG. 1. (a) Schematic view of the monoclinic unit cell of CDP in the FE phase (white prism). Two more formula units, one on top and the other on the right of the unit cell, are added to show the polarized chain in the b direction produced by the H_2 displacements. The arrows inside the dashed square frame show the relative atomic displacements for the FE mode. (b) Differential electronic charge-density $\Delta\rho(\mathbf{r})$ obtained as the system goes from the PE to the FE phase (see explanations in text). The 3D isosurface for $\Delta\rho(\mathbf{r})$ corresponding to a high isovalue ($\pm 0.2\ e\text{Å}^{-3}$) is shown. Black (pink) 3D contours show positive (negative) charge differences representing an increase (depletion) of charge after the transition. The zone displayed corresponds to that delimited by the dashed square in (a). (c) Idem as (b) for a smaller charge-density difference isovalue ($\pm 0.02\ e\text{Å}^{-3}$).

important [18,23]. Moreover, the interchain and Curie constant parameters of the model turn out to be smaller for DCDP than CDP, which is in contradiction with the isotope effect observed in the saturated polarization P_s [11]. Actually, the former magnitudes are expected to scale proportional to P_s^2 but P_s increases from 5.3 to 6.1 μC/cm^2 with deuteration [11,18]. In order to solve for this problem, Kojyo and Onodera improved the 1D model by considering two independent degrees of freedom: tunneling protons coupled to permanent dipoles that account for the spontaneous polarization. They could reproduce the isotope effect in the experimental dielectric and polarization data, and predicted an order-disorder phase transition in agreement with experiments [11]. However, due to the fact that these theories were developed at a rather phenomenological level, a confident and free-parameter analysis of the microscopic changes, energies, charge redistributions, and polarizations involved in the transition was not possible. These features may be analyzed by means of first-principles calculations, but to the best of our knowledge, no calculations of this type have been carried out in CDP or DCDP to study the PE-FE transition.

Recently, *ab initio* calculations based on the density functional theory (DFT) were conducted in KDP and its antiferroelectric (AFE) isomorph $NH_4H_2PO_4$ (ADP) [13,14,27–31]. It was found that significant instabilities arise only when the heavy atoms are allowed to relax with the protons, a fact that is in accordance with the experiments [13,14,32–35]. These instabilities are related to an effective electronic-charge redistribution that manifests inside the phosphates and along the H bonds in the FE transition of KDP [14,27,28,33]. The saturated polarization has the main contribution from the off-diagonal zx terms of the Born effective-charge tensors for the hydrogen atom and also some contribution from the corresponding diagonal terms for phosphorous [14,30]. On the other hand, first-principles calculations show that the stabilization of the AFE state in ADP is achieved through the optimization of the N-H-O bonds [29,31]. Tunneling and geometrical effects in these systems are coupled together in a self-consistent mechanism that leads to the huge isotope effect in agreement with experiments [9,13,14,36,37]. It is worth to mention here that other H-bonded systems recently discovered like some organic ferroelectrics where proton ordering is again intimately linked to ferroelectricity, could also have important tunneling and geometrical effects leading to the observed huge isotope effects [38,39]. Organic ferroelectrics have attracted much attention recently because they are potentially cheaper, less toxic and lighter than perovskite-type ferroelectrics usually used in technological applications [40]. In particular, croconic acid exhibits a large spontaneous polarization of $\approx$20 μC/cm^2, which is as large as that of $BaTiO_3$ at room temperature, suggesting that it could be a good candidate for organic electronic devices [41–43].

This work is devoted to the analysis of the microscopic mechanism that drives the PE-FE phase transition in CDP. To this end, we perform a first-principles study of the structures, energetics, charge redistributions, polarizations and isotope effects related to the phase transition. An important technical issue concerns the choice of exchange-correlation functional in the DFT calculations. This is because the potentials for proton/deuteron transfer in the H bonds are very sensitive to the O-O distance. Recently, it was found in some systems an overestimation of the H-bond strength and consequently an underestimation of the proton-transfer barrier when the van der Waals interactions were not considered in the *ab initio* calculations [16,44]. As a first step in this work, we present a detailed analysis of the performance of different exchange-correlation functionals in the H-bond geometry and energy barrier calculations using different *ab initio* methods. After this analysis, we choose the most adequate *ab initio* scheme for CDP, which was then used in the rest of the calculations. The paper is organized as follows: in Sec. II, we give details of the *ab initio* methods used. In Sec. III, we present and analyze the results obtained. Finally, in Sec. IV, we discuss and elaborate our conclusions.

II. AB INITIO METHODS

We have carried out first-principles calculations of CDP using the QUANTUM ESPRESSO (QE) program [45] and the VASP code [46,47], which work within the framework of DFT.

The QE program is based in a plane wave (PW) pseudopotential approach. In our calculations with this scheme, we considered nonlocal norm-conserving Troullier-Martins pseudopotentials [48] to integrate out the core electrons plus frozen ionic cores. The calculations were carried out using an automatic $7 \times 7 \times 7$ grid sampling of the electronic Brillouin zone. The plane-wave expansion was cut off at a maximum

PW energy of 110 Ry to obtain converged results when the short H-bond geometries were allowed to relax. In the case of $2 \times 3 \times 2$ supercell calculations of local FE instabilities performed with the short H-bond geometries fixed, we used a cutoff of 50 Ry, which yielded energies and geometries of sufficient accuracy.

The VASP calculations were carried out using projector augmented wave (PAW) potentials [49] and a plane wave basis set with a maximum energy cutoff of 900 eV. All the geometry optimizations were carried out until the forces on every mobile atom were smaller than 0.005 eV/Å. The Brillouin zone sampling was carried out according to the Monkhorst and Pack method [50] with a mesh $7 \times 7 \times 7$.

We use the experimental lattice constants for the PE [20] and FE [8] phases in the simulations for CDP and DCDP with each approach. It bears noting that no appreciable change with deuteration in the lattice dimensions for the FE phase is observed by neutron diffraction experiments [8]. In the PE phase of CDP, the H_2 hydrogens have two equilibrium positions equidistant to the middle of the H bond and separated by a distance δ [9]. Both positions are occupied by these protons with equal probability in the PE phase, and hence the averaged proton position is $\langle\delta\rangle = 0$. In our structural optimizations for the PE phase at $T = 0$, the positions of these hydrogens are fixed at the inversion symmetry site in the lattice, and we let all the rest of the atoms relax with the constraint that the H_2's remain centered in their H bonds [14,21,51,52]. In the optimizations for the FE structure, we perform full atomic relaxations that follow the pattern of the FE mode [see Fig. 1(a)] and lead to the ordered FE phase.

The performance of different exchange-correlation functionals for both methods are analyzed in detail in the next section.

The spontaneous polarization of the crystal was calculated using the Berry phase formalism [53–56] as implemented in the QUANTUM ESPRESSO program [45]. We have evaluated the polarization as the difference between the FE distorted structure and the reference PE phase. To avoid polarization quanta, a parametrized path of many intermediate structures between the PE and FE ones was considered at fixed cell [43,57,58]. The electronic contribution of the polarization is determined as a global Berry phase from products of Bloch states at neighboring k points of the Brillouin zone. The calculation is performed with strings of 20 k points extended along each of the three primitive reciprocal lattice vectors. The integration over the Brillouin zone is completed using up to 25 strings in k space. We have verified that these values for the k-point mesh yield converged results for the polarization.

III. RESULTS

A. Validation of the exchange-correlation functional and structural optimizations

In order to validate the *ab initio* scheme, we have used the VASP and QUANTUM ESPRESSO (QE) programs to perform structural optimizations of the PE and FE phases in CDP for different exchange-correlation functionals. We have compared the short H-bond geometry and long O-O distance results with experimental data. Additionally, we have calculated the energy barriers for the global proton transfer with each approach. These calculations were performed using several nonlocal van der Waals (vdW) functionals: vdW-DF [59–61], vdW-DF2 [62], optB88-vdW [60,63], and optPBE-vdW [60,63]. We have also applied the DFT-D2 scheme proposed by Grimme [64] as well as the approach of Tkatchenko and Scheffler [vdW(TS)] [65] to treat vdW interactions. In addition, the GGA Perdew-Burke-Ernzerhof (PBE) functional [66], which does not account for vdW long-range interactions, and a hybrid functional PBE0 [67] were also tested. The results are shown in Table I and compared with experimental data for CDP and DCDP. From here on, the label (QE) is added to the functional or DFT-scheme name to distinguish the QUANTUM ESPRESSO calculation from the VASP one.

Before proceeding with the analysis of the results of Table I, it is important to discuss some relevant aspects of these systems. It is observed experimentally that the O_1-O_2 distance of the long H bond is 0.06 and 0.08 Å larger than the O_3-O_4 one (short H bond) in the FE phase of CDP and the deuterated crystal DCDP, respectively (see Table I). The important consequence of this fact is that protons are always ordered in the long H bonds, which is in turn related to the nearly 1D character of the phase transition. On the other hand, the O_1-O_2 distance as well as the O_3-H_2 distance in the short H bond are not affected appreciably by deuteration. In contrast, the O_3-O_4 distance expands almost 0.03 Å with deuteration in the FE phase (Ubbelohde effect) as shown in Table I. It is worth to notice here that our first-principles calculations neglect nuclear quantum effects and correspond to infinite deuteron mass. However, in order to perform the validation of the *ab initio* scheme by comparing the calculated and measured short O-O distances, we need at least approximately to include nuclear quantum effects. To this aim, we perform Path Integral Monte Carlo (PIMC) [68] simulations of a three-site atomistic model for H bonds [69], which predicts successfully the universal H-bond geometry correlation in H-bonded complexes [70]. The model consists of a double-Morse potential for the hydrogen and an effective Morse potential for the O-O interaction [69]. We adjust the classical model parameters for the H bond in order to have a value of $\delta = 0.52$ Å, a short O-O distance of $\approx$2.53 Å, and a transfer energy barrier per particle of $\approx$53 meV, which correspond to an intermediate situation in CDP according to Table I. The PIMC simulations are well converged using $M = 128$ beads for the quantum polymer associated to each atom [69]. Further details of the model and calculations will be published elsewhere. The inclusion of the deuteron (proton) quantum dynamics in the model through the PIMC calculations leads to an O-O contraction for the short H bond of $\approx$0.03 (0.04) Å with respect to the classical case. Similar O-O contractions are observed when the deuteron (proton) nuclear dynamics is included in full *ab initio* calculations for some H-bonded solids with strong H bonds [16,71]. Thus, in order to perform the functional validation, we will consider a short O-O distance contraction of about 0.03 Å due to nuclear quantum effects when the *ab initio* data for this distance is compared with the corresponding experimental value for the deuterated lattice.

The results for the nonlocal vdW functionals, vdW-DF and vdW-DF2, and the dispersion scheme DFT-D2 show the largest energy barriers (see Table I). Particularly, the proton-transfer

TABLE I. *Ab initio* results for the global energy barriers and H-bond structural parameters in the PE and FE phases for several exchange-correlation functionals and DFT methods mentioned in the main text, calculated with VASP and QUANTUM ESPRESSO (QE). Also shown are the experimental H-bond parameters (Expt.) for the FE phase [8] in CDP and DCDP and for the PE phase in CDP [20] and DCDP [78]. Distances are in angstroms.

DFT	FE			PE	Energy Barrier
Methods	$d(O_3\text{-}O_4)$	$d(O_3\text{-}H_2)$	$d(O_1\text{-}O_2)$	$d(O_3\text{-}O_4)$	(meV/f.u.)
vdW-DF	2.587	1.022	2.557	2.428	69
vdW-DF (QE)	2.570	1.027	2.598	2.429	55
vdW-DF2	2.597	1.018	2.563	2.431	95
vdW-DF2 (QE)	2.590	1.021	2.591	2.439	85
opt-B88-vdW	2.512	1.051	2.529	2.419	37
opt-PBE-vdW	2.537	1.038	2.542	2.420	44
PBE	2.478	1.061	2.517	2.408	9
PBE (QE)	2.501	1.065	2.560	2.419	8
vdW(TS)	2.478	1.063	2.508	2.407	29
vdW(TS) (QE)	2.513	1.057	2.571	2.425	32
PBE0	2.473	1.039	2.528	2.383	22
PBE0 (QE)	2.508	1.039	2.580	2.397	23
DFT-D2	2.500	1.056	2.509	2.411	52
DFT-D2 (QE)	2.535	1.052	2.545	2.421	65
DCDP (Expt.)	2.509	1.006	2.569	2.50	-
CDP (Expt.)	2.483	1.001	2.563	2.46	-

energy barriers and short H-bond geometries obtained with vdW-DF2 are similar to the corresponding values calculated for squaric acid (SQA) with the same scheme [16], in spite of the different chemical units that connect the H bonds in both compounds. However, one should expect substantially different values for the global proton-transfer energy barriers for both compounds since SQA has a $T_c \approx 2.5$ times larger than that of CDP [72]. Calculated low values of T_c in SQA could be originated in an underestimation of the proton-transfer energy barriers or the simplification of the models used [16,17]. On the other hand, our calculations with vdW-DF and vdW-DF2 of the O_3-O_4 distances for DCDP using VASP (QE) including nuclear quantum corrections are ≈2.56 Å (2.54 Å) and 2.57 Å (2.56 Å), respectively. These values are in general comparable and not much smaller than the calculated O_1-O_2 distances, in contradiction with experiments (see Table I). For instance, in the case of vdW-DF2 (QE), the difference between the short and long H-bond distances is almost half that of the experiment. Moreover, the corrected O_3-O_4 distances for the vdW-DF and vdW-DF2 schemes using VASP (QE) turn out to be ≈0.05 Å (0.03 Å) and 0.06 Å (0.05 Å) larger, respectively, than the experimental result for DCDP. Comparing the performance of the optB88-vdW functional respect to the other nonlocal functionals, we find smaller energy barriers and considerably shorter O_3-O_4 distances, as shown in Table I. In this case, we expect somewhat stronger quantum effects leading to O_3-O_4 distances much shorter than the experimental values. The use of optPBE-vdW would lead to structural parameters close to experimental values after the nuclear quantum corrections, but with a considerably lower barrier than those obtained with the other nonlocal functionals and the DFT-D2 scheme. Therefore, the use of nonlocal vdW functionals does not seem to be convenient for an *ab initio* calculation in CDP.

On the other hand, the performance in our *ab initio* calculations for CDP of functionals that neglect vdW interactions like PBE is worse than that of nonlocal functionals, as can be deduced from Table I. The inclusion of nuclear quantum effects in the PBE calculation would result in very short O_3-O_4 distances and consequently very low energy barriers. The hybrid functional PBE0 does not improve too much the situation, showing results for the O-O distances similar to those obtained with PBE (see Table I).

The use of the DFT-based dispersion scheme DFT-D2 (QE) that includes pairwise-additive vdW corrections to the total energy [64] substantially improves the scenario. First, it gives energy barriers comparable to the results of more complex nonlocal approaches. Second, the O_3-O_4 distance obtained after nuclear quantum corrections, ≈2.50 Å, is in very good agreement with the experimental result for DCDP. Moreover, the calculated difference between the corrected short O-O distance and the long one amounts to ≈0.04 Å, which is in fair agreement with the experimental difference of ≈0.06 Å (see Table I). On the other hand, the results for the vdW(TS) approach show smaller O_3-O_4 distances and much smaller energy barriers than the results for DFT-D2.

Comparing the results obtained with VASP and QE for each functional in Table I, we observe differences in the O-O distances and the energy barriers which may be attributed to the different pseudopotentials used. More specifically, the QE calculations give somewhat larger O-O distances for the long H bond than VASP ones. Similar trends are observed for the O-O distances of the short H bond in all the schemes although for the nonlocal functionals the situation is inverted. The maximum difference observed in the O_3-O_4 distance is about 0.03 Å, which is an order of magnitude smaller than the maximum dispersion in the values of the O_3-O_4 distances for the different functionals (≈0.12 Å, see Table I). However, this maximum

TABLE II. *Ab initio* (PW) results obtained with DFT-D2 (QE) for the internal structure parameters of the PE and FE phases considered in the text. Available data from neutron diffraction (ND) and x-ray experiments are added for comparison for the PE phase (CDP) at room temperature (RT) and the FE phases of CDP at 80 K and DCDP at 83 K. We also show in parenthesis the theoretical parameters for the short H-bond geometry in the FE phase obtained after correcting the *ab initio* results with a phenomenological model calculation that accounts for nuclear quantum effects (see explanations in text). Distances in angstroms and angles in degrees.

	PE structure			FE structure		
Structural parameters	PW	ND [20] (RT)	X ray [81] (RT)	PW	ND (DCDP) [8] (83 K)	ND (CDP) [8] (80 K)
d(P-O_1)	1.610	1.574	1.566	1.616	1.569	1.579
d(P-O_2)	1.528	1.484	1.481	1.530	1.508	1.503
d(P-O_3)	1.577	1.531	1.529	1.613	1.569	1.569
d(P-O_4)	1.577	1.531	1.529	1.545	1.504	1.508
d(O_1-H_1)	1.021	0.995	0.9	1.029	1.006	1.007
d(O_3-H_2)	1.230	1.00	1.236	1.052(1.09)	1.031	1.029
d(O_1-O_2)	2.525	2.521	2.537	2.545	2.569	2.563
d(O_3-O_4)	2.421	2.46	2.472	2.535(2.50)	2.509	2.483
δ	0	0.48	0	0.431(0.32)	0.447	0.425
<O_1-P-O_2	105.8	107.4	107.3	107.6	107.1	107.2
<O_1-P-O_3	107.2	106.2	106.1	102.4	102.1	102.1
<O_3-P-O_4	110.2	106.2	106.1	110.1	109.7	109.5
<O_3-H_2-O_4	179.5	174.0	180.0	177.0	180.0	180.0
<O_1-H_1-O_2	174.3	173.2	166.0	172.0	173.2	172.9

difference produced by the use of different pseudopotentials is of the order of the nuclear quantum correction. Therefore, an extensive validation of different *ab initio* schemes in calculations for these systems as the one performed in this work is preferable in order to minimize the errors in the approximations.

The calculated short O-O distances in the PE phase show systematically lower values than the experimental results for all the DFT schemes studied, as shown in Table I. The deviations would be even larger if nuclear quantum effects are included because quantum effects produce a bond contraction in symmetric H bonds. There is also a small dispersion between the different values for each approach. The disagreement with the experiment in this case is mainly attributed to the static optimization for centered protons in the H bonds, although it could be partially originated in the approximate character of the exchange-correlation functional [14,73].

The comparative analysis of the different *ab initio* schemes made in the paragraphs above shows that DFT-D2 (QE) is the most adequate approach for an *ab initio* calculation in CDP. From here on, all the calculations in this work are performed with DFT-D2 (QE) unless we state the contrary.

The structural results for the optimization of the PE and FE phases of CDP using the chosen *ab initio* scheme are shown and compared to the experiments in Table II. The overall agreement with experiment is good although the O_3-H_2-O_4 distance in the PE phase is too short as discussed above and the P-O distances are rather overestimated in both phases. The observed O-O contraction in the PE phase for centered protons is similar to the corresponding result obtained in recent *ab initio* calculations for KDP [14]. On the other hand, the degree of PO_4 distortion associated with the proton ordering in the FE phase, d(P-O_3) − d(P-O_4), is well reproduced (see Table II).

B. Charge-density redistributions and saturated polarization

We now turn to the analysis of the charge redistributions produced by the H_2 off-centering to shed light on the microscopic mechanism of the phase transition. To this aim, we start from the PE phase with the H_2 atoms centered and relax all atoms with the constraint that the O ions remain fixed in their positions. This leads to a polarized (PO) structure where the H_2 atoms are off-centered in the O-H-O bonds and the PO_4 distorts in a similar way that happens in the true FE phase. Therefore, maintaining the O-O distances fixed enables us to compute the charge density difference $\Delta\rho(\mathbf{r}) = \rho_{\mathrm{PO}}(\mathbf{r}) - \rho_{\mathrm{PE}}(\mathbf{r})$, which gives us qualitative information about the microscopic changes affecting the phase transition [14,27]. We show representative isosurfaces of this differential charge in the three dimensional plots of Figs. 1(b) and 1(c). We observe as the H_2 atom displaces towards the O_3 atom an increase in the charge localized in the O_3-H_2 bond, while there is a depletion of the charge around the $O_4 \cdots H_2$ bond [See Fig. 1(b)]. This is in agreement with the respective bond distortions observed in the FE phase (see Table II). Next in importance is a charge increase (decrease) in the P-O_4 (P-O_3) bond of the phosphate [see Fig. 1(c)]. Thus there is a net charge flow from the O_3 to the O_4 side of the phosphate which is in accordance to the phosphate distortion observed in the FE phase (see the increase and decrease of the P-O_3 and P-O_4 bond distances, respectively, in Table II). This charge flow mechanism gives rise to an electronic polarization of the phosphates along the b direction in the FE phase. The behavior of the charge reorganization along the chains in CDP resembles that found in the phosphates plus acid H-bond subsystems of KDP and ADP, which pertain to a more complex 3D H-bonded network [14,27,29,31].

We have evaluated the saturated polarization of CDP with the DFT-D2 (QE) scheme using the Berry phase method [53,54] as explained in Sec. II. Thus we have calculated

the polarization difference between the fully relaxed FE structure and the reference PE one, whose internal parameters are listed in Table II. We obtain a value of 5.4 μC/cm^2 for the spontaneous polarization in the b direction and negligible values for the projections onto the a and c axes of the monoclinic cell. This is in very good agreement with the experimental value of 5.3 μC/cm^2 measured along the b axis in Ref. [18].

We have also determined the influence of different *ab initio* schemes in the calculated saturated polarization. The use of the PBE (QE) scheme leads to a value of 5.6 μC/cm^2 for P_s in the b axis, very similar to that for the DFT-D2 (QE) approach. However, in the case of nonlocal van der Waals corrections the calculated values of P_s in the b direction are much larger: 6.4 and 7.4 μC/cm^2 for vdW-DF (QE) and vdW-DF2 (QE), respectively. These larger values could be related to the different equilibrium geometries found in the short H bond for these functionals, i.e., larger polar distortions compared to the PBE and DFT-D2 approaches (see Table I), which in turn may enhance the electronic-charge redistributions [43]. The maximum percentage change in P_s between these schemes is $\approx$27%, which is similar to the corresponding relative change ($\approx$25%) found between PBE, DFT-D2, and different hybrid functionals in the calculation of P_s for croconic acid [43].

In order to account for the different atomic contributions to the polarization P_s, we have also determined the dynamical Born effective-charge tensors Z^*_{ij} for each atomic species using DFT linear response as implemented in QUANTUM ESPRESSO [74]. These effective charges are defined as the derivative of the polarization vector with respect to atomic displacements. Hence, P_s is determined as the sum of the matrix products between the atomic charge tensors and the atomic displacement vectors from the PE to the FE configurations. With this procedure, we are able to discriminate the contributions to the total polarization of the different atoms [14,30]. The value of the saturated polarization calculated with this method is similar to that obtained with the Berry phase formalism.

We observe that the most important contribution to the polarization arises from the Born effective-charge tensor associated to the H_2 atoms. The largest term for this atom, which comes from the off-diagonal value of its effective charge $Z^*_{yx}(H_2) = 1.6e$ and its large displacement along the a direction, accounts for 70% of the total polarization. There is also a diagonal contribution from H_2 which represents 15% of P_s due to the projected displacement in the b direction and the charge-tensor component $Z^*_{yy}(H_2) = 0.8e$. Thus these two terms are responsible for 85% of the cell polarization. The remaining 15% comes mainly from the net polarization of the phosphates with the most important contribution arising from the diagonal effective charge of phosphorus, $Z^*_{yy}(P) = 2.3e$. On the other hand, O_3 screens partially the phosphorous contribution and contributes negatively to the total polarization. O_1, O_2, O_4, H_1, and Cs have negligible contributions to P_s.

C. Global and local FE instabilities, tunneling, and geometrical effects

It is observed that the main structural effect of deuteration in CDP is the increase of the O_3-O_4 distance and the parameter δ [8]. This is the well known Ubbelohde (or geometrical) effect [10,71,75,76], which is verified in the members of the KDP-type family of compounds [9,16,72]. The deuterated lattice is also somewhat expanded in the PE phase, mainly in the b direction [77], although there is no appreciable lattice-parameter change with deuteration in the FE phase [8]. Here we mimic the effect of deuteration in the PE phase by considering increasing O_3-O_4 distances in the lattice. Thus, we perform global optimizations at different fixed O_3-O_4 distances and determine the relative variations on the parameter δ and the effective energy barriers. We present total energy calculations for the following representative cases (i) $d(O_3 - O_4) = 2.46$ Å, which is the measured value for CDP [20]; (ii) $d(O_3 - O_4) = 2.50$ Å, corresponding to the measured value for DCDP [78]; and (iii) an intermediate value $d(O_3 - O_4) = 2.48$ Å. The global distortions are carried out in two steps: (i) considering H_2 displacements alone, and (ii) also allowing for the concomitant relaxation of the P, Cs, and H_1 atoms. In Fig. 2, we plot the total *ab initio* energy as a function of the FE mode amplitude represented by a collective coordinate, which coincides with the proton off-centering displacement $\delta/2$ along the disordered O_3-H_2-O_4 bonds.

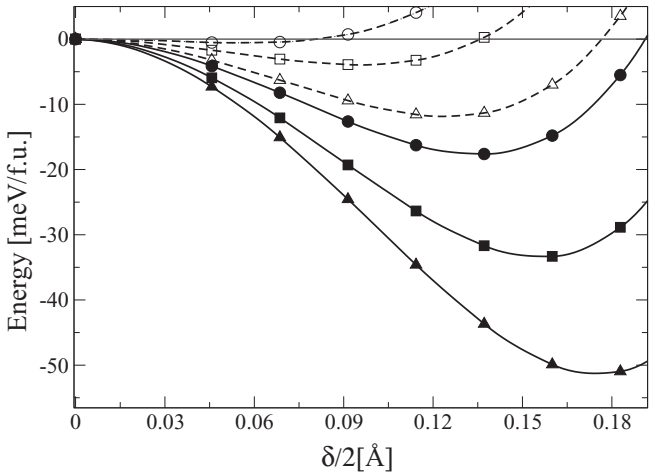

FIG. 2. Energy profiles of the global FE instability as a function of $\delta/2$ for different values of $d(O_3$-$O_4)$: 2.46 Å, corresponding to CDP (circles), 2.48 Å (squares), and 2.50 Å, which corresponds to DCDP (triangles). Empty symbols and dashed lines indicate that only H_2 atoms displace. Motions that also involve P, Cs, and H_1 atoms are represented by filled symbols and solid lines. Lines are guides to the eye only.

We observe in Fig. 2 that the global FE instabilities grow as the O_3-O_4 distance increases in CDP. They are even larger if the heavier ions P and Cs, and the H_1 atom are included in the distortions. For $d(O_3 - O_4) = 2.46$ Å, which corresponds to the CDP case, a very tiny double-well develops if the protons alone are displaced. If we allow for the relaxation of the heavier atoms the barrier is much larger, $\approx$18 meV per formula unit (f.u.), and the distance between proton minima in the bond amounts to $\delta = 0.27$ Å (see Fig. 2). This global energy profile is similar to that obtained *ab initio* for KDP, where the energy barrier per proton is $\approx$19 meV and $\delta = 0.3$ Å [52]. The expansion of the O-O bond mimicking the effect of deuteration to $d(O_3 - O_4) = 2.50$ Å (DCDP case) leads to an effective energy barrier for polarization inversion of $\approx$52 meV/f.u. as

can be seen in Fig. 2. It also produces a substantial increase of ≈29% for δ. Unfortunately, to the best of our knowledge, there is no available experimental data on the distance δ in the PE phase of DCDP to compare with our calculations. On the other hand, the Ubbelohde effect is also observed in the expansion of the O_3-O_4 distance with deuteration in the FE phase, which amounts to $\Delta_{OO} \approx 0.026$ Å (see Table II). Concomitantly to this expansion, the parameter δ increases from 0.425 to 0.447 Å with deuteration as shown in Table II. Now, we fix the (O_3-O_4) distances to the corresponding measured values in the FE phase, $d(O_3 - O_4) = 2.483$ and 2.509 Å, for CDP and DCDP, respectively (see Table II). Then, we perform global relaxations and obtain the values $\delta = 0.35$ and 0.39 Å, for CDP and DCDP, respectively. The obtained parameters appear somewhat underestimated when compared to the experiments but their difference, $\Delta\delta \approx 0.04$ Å, is in qualitative agreement with the geometrical effect of deuteration observed. Our results for δ, the increase with deuteration $\Delta\delta$, and the energy barriers per particle in CDP and DCDP are similar to the corresponding values obtained by *ab initio* calculations in KDP and DKDP [52].

The order-disorder character of the FE transitions is reflected in the proton double-occupancy observed in the family of H-bonded ferroelectric compounds.[9,79] The double-site distribution can be ascribed either to thermal proton disorder, or to tunneling along the H bond, or even to both of them. Each of these possibilities are related to local instabilities produced by correlated proton distortions plus heavy ion displacements along the FE pattern of motion [see Fig. 1(a)]. We now address this issue by performing *ab initio* calculations of localized FE distortions and considering increasingly larger clusters embedded in a host PE matrix of CDP [20]. We take large $2 \times 3 \times 2$ supercells of the PE matrix with fixed O atoms and centered protons, and perform cluster distortions including up to $N = 4$ H_2's along the disordered chain in the b direction [see Fig. 1(a)]. The maximum cluster size of $N = 4$ protons along the b chain ensures that the clusters are isolated in the supercells considered subjected to periodic boundary conditions. As in the case of global displacements, we consider here two cases for the cluster distortions: (i) motions of disordered protons (deuterons) alone and (ii) also including relaxations of P, Cs, and H_1 atoms. We assume equal and linear displacements along bonds of the H_2 atoms inside the clusters for simplicity [13,14]. With the purpose to determine the onset of tunneling, we solve the Schrödinger equation for each cluster motion at fixed potential considering an effective cluster mass as was done in Ref. [14]. In order to analyze the main effect of deuteration, we also perform similar calculations in a structure with the O_3-O_4 distance expanded to 2.50 Å (DCDP) and with the deuteron-cluster masses for the quantum calculation. For example, the effective cluster mass per deuteron for the $N = 4$ D cluster for case (ii) amounts to $\mu_D = 3.8$ proton masses.

The *ab initio* energies for clusters of different sizes are plotted as a function of the local coordinate $x \equiv \delta/2$ for CDP in Fig. 3(a). The cluster displacements of protons alone (up to $N = 4$) do not produce instabilities in CDP. The concomitant relaxation of the atoms P, Cs, and H_1 leads to a double well with an energy barrier of ≈24 meV in the case of $N = 4$ protons. Only in this case the quantization of the local motion

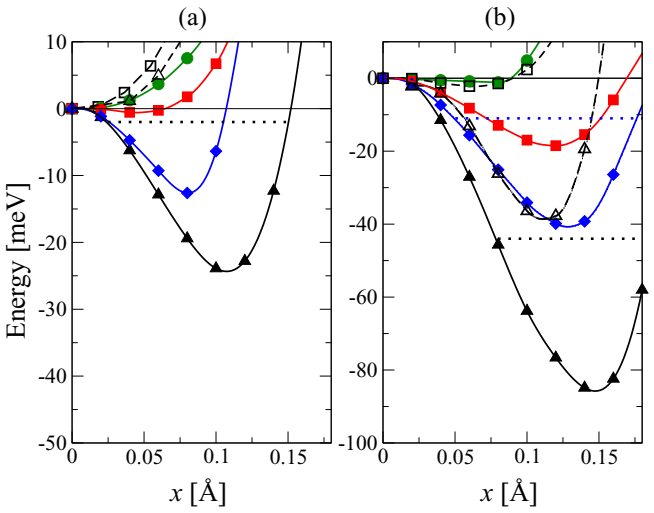

FIG. 3. Energy profiles for correlated local distortions in (a) CDP and (b) DCDP as a function of the local coordinate $x \equiv \delta/2$. Reported are clusters of $N = 1$ H(D) (circles), $N = 2$ H(D) (squares), $N = 3$ H(D) (diamonds), and $N = 4$ H(D) (triangles). Empty symbols and dashed lines indicate that only the $H_2(D_2)$ atoms displace. In this case, only the curves corresponding to clusters of $N = 2$ H(D) and $N = 4$ H(D) are shown. Motions that also involve P, Cs, and H_1 atoms relaxations are represented by filled symbols and solid lines. Negative ground-state energies signaling tunneling for the $N = 4$ H, $N = 3$ D, and $N = 4$ D clusters are shown by dotted lines. Lines are guides to the eye only.

at fixed potential leads to a ground-state level below the top of the barrier at ≈−2.1 meV indicating signatures of tunneling. Thus the FE correlation length is approximately two unit cells (4 formula units) [14].

The situation changes substantially when the cluster distortions are computed in the lattice with the O_3-O_4 distance increased to 2.50 Å (DCDP). We observe in Fig. 3(b) larger instabilities for all cases. However, in most cases, the quantum calculations lead to energies above the barrier. Only in the cases of $N = 3$ and 4 deuterons, with the concomitant relaxation of the heavy atoms plus H_1, we observe signatures of tunneling. The ground-state energies in these cases lie below the top of the barrier at ≈−11.9 and −44.3 meV for the $N = 3$ and 4 D clusters, respectively, as shown in Fig. 3(b).

In order to investigate the existence of coherent and incoherent tunneling for these clusters and the crossover to a classical regime with T [80], we have computed the position and momentum distributions, $n(x)$ and $n(p)$, respectively, at different temperatures. The existence of a node in the momentum distribution of a system that presents bimodal position distribution is a signature of coherent ground-state tunneling [14,36,80]. These distributions are determined using the density matrix formalism [80] with the information of the wave functions and energy eigenvalues that results from the solution of the Schrödinger equation for each cluster.

The calculated distributions $n(x)$ and $n(p)$ are shown for several temperatures in Figs. 4(a) and 4(b), respectively, for the $N = 4$ H cluster with heavy atom relaxations [case (ii)]. The distributions for the $N = 3$ D cluster in case (ii) are shown in Figs. 5(a) and 5(b). It is important to remark that these

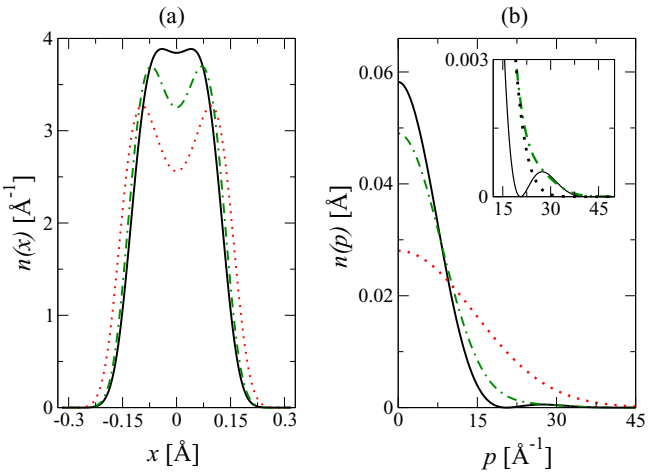

FIG. 4. Position (a) and momentum (b) distributions for a cluster of $N = 4$ protons in CDP with concomitant relaxations [case (ii), see explanations in text] at different temperatures. Black solid line: 7 K, green dotted-dashed line: 153 K, and red dotted line: 700 K. A Gaussian fit (black dotted line) to the momentum distribution at 153 K (green dotted-dashed line) is shown in the inset of the right panel together with the curve at 7 K (black solid line).

clusters are immersed in a mean-field host PE matrix and the physical situation corresponds to temperatures above the T_c of the system (≈150 and ≈260 K for CDP and DCDP, respectively). However, we will also analyze their behavior at lower temperatures for illustrative purposes. We observe a double peak distribution for $n(x)$ at all temperatures considered denoting barrier crossings in both clusters even at very low T [see Figs. 4(a) and 5(a)]. To discriminate whether tunneling exists or not we have to look at $n(p)$. Figures 4(b) and 5(b) show that a node is present in $n(p)$ at 7 K indicating coherent tunneling for both clusters in the ground state (see also the insets to these figures) [14]. The node and the associated oscillation at larger p gradually fade out with increasing temperature in both clusters [see, for instance, the curves at $T = 7$ and 60 K in the inset to Fig. 5(b) for the $N = 3$ D cluster]. This happens because the ground state is mixed with the first excited state as the temperature is increased. In the case of the $N = 4$ H cluster, the small oscillation with a maximum at $p \approx 28$ Å^{-1} remains up to temperatures of ≈100 K. For the $N = 3$ D cluster, the corresponding oscillation dissapears at lower T (≈80 K) because the tunnel splitting is smaller.

Let us now analyze the $N = 4$ H cluster at $T = 153$ K, which corresponds to the physical situation in the PE phase of CDP. The first-excited state population reaches ≈16% at this T while the ground state one is still high (≈84%). The small oscillation in $n(p)$ is no longer present at this temperature as shown in Fig. 4(b). However, the distribution is non-Gaussian with an extended tail. This is better visualized in the inset to Fig. 4(b), where this curve is compared to a Gaussian fit. The observed mixed-state for the cluster and the form of the $n(p)$ distribution now suggest the existence of incoherent tunneling [80]. As the temperature is further increased there is a crossover to a classical regime where the distribution becomes Gaussian and thermal hopping plays a preponderant role. This shape is observed for the distribution at 700 K, as shown in Fig. 4(b). Similar behavior of the proton momentum distributions were obtained with model and full-quantum calculations in high-pressure phases of ice [80].

The analysis of the $n(p)$ distribution for the $N = 3$ D cluster at $T = 263$ K (PE phase of DCDP) reveals the existence of a subtle non-Gaussian tail (see the corresponding curve in Fig. 5(b) and its comparison with a Gaussian fit in the inset). This indicates that mixed-state incoherent tunneling still plays some role in this case, although less important than the role of incoherent tunneling for the $N = 4$ proton-cluster dynamics in CDP near the critical temperature.

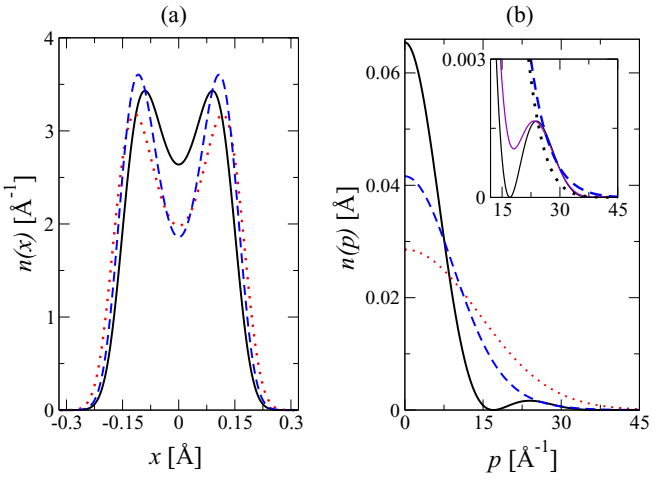

FIG. 5. Position (a) and momentum (b) distributions for a cluster of $N = 3$ deuterons in DCDP with concomitant relaxations [case (ii), see explanations in text] at different temperatures. Black solid line: 7 K, blue dashed line: 263 K, and red dotted line: 700 K. A Gaussian fit (black dotted line) to the momentum distribution at 263 K (blue dashed line) is shown in the inset of the right panel together with the curves at 7 K (black solid line) and at 60 K (magenta solid line).

IV. DISCUSSION AND CONCLUSIONS

We have performed a comprehensive study of the global energy barriers and H-bond geometries in CDP in order to validate different functionals and *ab initio* schemes including or not van der Waals interactions. The resulting energy barriers from the different first-principles schemes were compared between each other, while the H-bond geometry results were compared to experimental data of CDP and DCDP. The short H-bond geometry was corrected with a result of a phenomenological quantum model to account for the O-O contraction produced by the quantum nature of the light nuclei (Ubbelohde effect). After a careful analysis, we have arrived to the conclusion that DFT-D2 (QE) gives the best general performance among all the studied schemes.

The equilibrium structures for the PE and FE phases of CDP which result from the described first-principles calculations with DFT-D2 (QE) are in general good agreement with the available experimental data. In particular, most of the parameters for the long and short H-bond geometries measured in both phases are well reproduced by our *ab initio* calculations. The small overestimation observed in the theoretical P-O distances, as well as the underestimation in the O_3-O_4 distance in the PE phase, are also found in calculations for KDP [14]. The

latter discrepancy can be ascribed to the constrained technique to simulate statically the PE phase. However, the approximate character of the exchange-correlation functionals could be also related to the mentioned differences.

The release of the constraint for H_2 to remain in the middle of the H bond in the PE phase produce atom distortions, which follow the FE mode pattern as depicted in Fig. 1(a). Our *ab initio* calculations show that this pattern is mainly composed by H_2 displacements along the H bonds forming chains in the *b* direction. These distortions are three times larger than the largest displacement of the other atoms in the FE mode. This feature, together with the relevance of the off-diagonal *yx* terms in the effective charge tensors of H_2 as revealed by linear response calculations, yield to the fact that this atom has the most important contribution to the total FE polarization. This is in accordance with the qualitative picture obtained by the analysis of the charge redistributions in the FE distortion. In this regard, the isosurface with the largest isovalue for the charge-density difference produced by the FE distortion is that found along the short H bonds as shown in Fig. 1(b).

Next in importance for the charge redistributions are other contributions to the FE mode which come from the P atom and the O_3-P-O_4 bond distortions. These modifications result in a local electronic charge transfer inside the phosphates as shown in Fig. 1(c). The electronic charge in this case flows from the P-O_3 to the P-O_4 bond with a concomitant tetrahedron distortion, that is, the P-O_4 bond strengthens while the P-O_3 bond weakens, as can be observed in Table II. This charge transfer produces a local dipole that contributes to the spontaneous polarization along the *b* direction, although this contribution is less significant than that of the H_2 atom shown in Fig. 1(b). The quantitative analysis of the different atom contributions to the total polarization performed with the help of the effective-charge tensors corroborates these conclusions. On the other hand, the P-O_1 and P-O_2 bonds do not distort and no charge transfer is observed in this side of the phosphate [see Fig. 1(c)]. These bonds form, together with the long O_1-H_1-O_2 bonds which are ordered at any temperature, chains that run perpendicular to the FE *b* axis.

Our *ab initio* result for the spontaneous polarization of CDP is in very good agreement with the experimental value. On the other hand, it is observed experimentally that KDP and CDP show similar magnitudes for P_s [18,19]. It is worth to notice here that we find close similarities in the microscopic FE behavior when our present results are compared with those from recent *ab initio* calculations in KDP [14,30]. The main contribution to the polarization in CDP comes from a nondiagonal effective-charge component of H similarly to what happens in KDP [14,30]. Also, the H displacements and the changes in P-O distances produced by the FE distortion are similar in both compounds. Moreover, the charge transfer mechanism driven by the FE distortion in CDP involves mainly a charge redistribution along the short H bonds and also inside the phosphates, similarly to the corresponding behavior found in KDP [14,27]. However, the phosphate distortions and charge transfers involve the whole tetrahedron in KDP, while in CDP only half part of the phosphate distorts and contributes to the polarization [see Fig. 1(c)]. Considering that half protons contribute to the total polarization in CDP compared to the KDP case, and that both compounds have similar volumes per formula unit, one question naturally arises: why do both materials manifest almost identical values for P_s? This behavior can be explained by the large value of the nondiagonal component $Z^*_{yx}(H_2)$ obtained in our calculations for CDP. This magnitude is $\approx$2.7 times larger than the component $Z^*_{zx}(H)$ responsible of $\approx$60 % of the total polarization in KDP [14,30].

The calculated energy curves for global FE distortions show that the barriers for the polarization inversion are significant only when the protons are relaxed accompanied by the heavier atoms. The overall similarity found for the global instabilities in CDP and KDP [52] is in accordance with the close values measured for their critical temperatures [8,9]. The effect of deuteration, simulated by the increase in the O-O distance in the lattice, leads to larger barriers for the polarization inversion and larger distances between deuteron minima. We observe that the increases in the energy barriers and δ with deuteration in CDP are very similar to the corresponding behavior for KDP [52]. This is possibly correlated with the close values for the critical temperature increase caused by deuteration that are measured in both systems ($\Delta T_c \approx 110$ K).

The analysis of local FE distortions inside a PE matrix reveals the existence of strong FE correlations existing along the chains in the *b* direction [see Fig. 1(a)], which are in accordance with the anisotropic correlations measured by neutron scattering experiments [22]. As a general feature, our calculations show that the instabilities grow with the cluster sizes, with the inclusion of heavy atoms relaxations, and also with increasing O-O distance. In CDP, the barriers are small enough that for most of the cluster sizes analyzed the quantum ground states have energies above the top of the barrier. However, in the case of $N = 4$ protons plus heavy-atoms distortions, the ground state lie just below the top of the barrier signaling tunneling for this cluster. This is corroborated by an analysis of the cluster momentum distributions at different temperatures, which lead to the conclusion that this cluster allows for incoherent tunneling near T_c in the PE phase of CDP. The onset of tunneling at a critical cluster size provides a rough indication of the correlation length. Hence the FE correlation length in CDP should be about four formula units in the disordered phase. The situation in DCDP is different with stronger instabilities and correlation lengths accordingly shorter. Up to the cluster sizes analyzed, tunneling arises for clusters comprising at least three deuterons (and associated heavy-atom distortions), which is confirmed by momentum-distribution calculations. Therefore the simple picture of a proton tunneling alone in the H bond proposed by the tunneling model [12] is not supported by our calculations for CDP or DCDP. The overall qualitative behavior of the local energy profiles as well as the quantum behavior of the clusters are qualitatively similar to the results found in *ab initio* calculations for KDP and DKDP [13,14]. The present *ab initio* calculations for CDP and DCDP, as well as those performed for KDP, ADP, and their deuterated counterparts, [13,14,29,31] lead us to the conclusion that the observed proton double occupancy in these systems can be explained by the tunneling of large and heavy clusters. This is in accordance with measurements of double-site distributions for the P atoms in H-bonded ferroelectrics [34,35].

The momentum distributions for the proton(deuteron) motion in KDP(DKDP) have been determined experimentally

by neutron Compton scattering experiments [36,37]. These experiments reveal quantum coherence in the PE phase of KDP, but an apparent lack of coherence in the PE phase of DKDP. It is speculated that this behavior is a consequence of smaller tunnel splittings $\Delta E_{\rm ts}$ for DKDP than for KDP in such a way that the relation $kT \gg \Delta E_{\rm ts}$ is fulfilled in the PE phase of DKDP and no coherence is observed. In line with this idea, we observe that the $N = 3$ D cluster in DCDP displays weak incoherent tunneling features because $\Delta E_{\rm ts} \approx 167$ K is smaller than T_c. Moreover, the $N = 4$ H cluster in CDP has a tunnel splitting $\Delta E_{\rm ts} \approx 252$ K which is larger than T_c, and hence the signal of incoherent tunneling is stronger near the transition. On the other hand, the comparison of the widths of the momentum distributions in KDP and DKDP measured by neutron Compton scattering experiments indicates that there must be a compensating softening of the effective potential in DKDP [36,37]. It is concluded that there is a mass-dependent quantum coherence length in these systems which decreases with increasing mass. This is in accordance with recent *ab initio* calculations in KDP and DKDP that demonstrate a shrinking of the correlation and coherence length with deuteration [13,14]. Our current results for CDP and DCDP give also support for this idea.

The effects of thermal fluctuations in the PE phase near the FE transition are difficult to evaluate since *ab initio* molecular-dynamics calculations are not computationally feasible for a sufficient large system. We speculate that the PE scenario would be composed of clusters of different sizes competing thermally with different tunneling probabilities. As the FE transition approaches larger clusters having vanishing tunnel splittings would prevail [14]. In this situation, quantum effects produced by isotopic substitution at fixed potential were found to be rather modest in DKDP [13,14]. However, nonlinear feedback effects between tunneling and geometrical modifications largely amplify the quantum effects. In the end, the geometrical effect dominates the scenario and accounts for the huge isotope effect in agreement with experiments [9,13,14,79]. The trends for the local cluster energetics obtained in this work, being similar to those found in KDP and DKDP, enable us to speculate that this nonlinear mechanism could also explain the huge isotope effects in CDP and DCDP.

In summary, we have performed for the first time *ab initio* calculations to analyze the microscopic mechanism behind the PE-FE phase transition in CDP. The structural results for both phases are in good agreement with experiments. Our first-principles result for the saturated polarization is in remarkable accordance with the experimental value. The analysis of the different atomic contributions to P_s shows that the nondiagonal yx component of the effective-charge tensor of H_2 is the main responsible of the total FE polarization along the b axis. Its large value, more than twice the nondiagonal zx component of the Born charge for hydrogen in KDP, may explain the close values for P_s measured in both compounds in spite that for CDP only half protons in the polarization units are involved in the transition. This behavior is also consistent with the charge density redistributions observed along the disordered H bridges and inside the phosphates in both systems [14,27]. The study of global and local FE correlations shows that the energy barriers are much larger and the length scales accordingly much shorter when the protons are accompanied by heavy atoms distortions. Moreover, we observe that the quantum coherence is produced by a dressed proton(deuteron) and that the quantum coherence length in the system decreases with deuteration in agreement with experiments and *ab initio* results obtained in other H-bonded ferroelectrics.

ACKNOWLEDGMENTS

We thank J. Kohanoff and F. Torresi for helpful discussions. We acknowledge support from Consejo Nacional de Investigaciones Científicas y Técnicas (CONICET), Argentina.

[1] M. E. Lines and A. M. Glass, *Principles and Applications of Ferroelectric and Related Materials* (Clarendon, Oxford, 1977).
[2] C. E. Botez, J. D. Hermosillo, J. Zhang, J. Qian, Y. Zhao, J. Majzlan, R. R. Chianelli, and Cristian Pantea, J. Chem. Phys. **127**, 194701 (2007).
[3] H. Lee and M. Tuckerman, J. Phys. Chem. C **112**, 9917 (2008).
[4] S. M. Haile, C. R. I. Chisholm, K. Sasaki, D. A. Boysena, and T. Udaa, Faraday Discuss. **134**, 17 (2006).
[5] J. Otomo, T. Tamaki, S. Nishida, S. Q. Wang, M. Ogura, T. Kobayashi, C. J. Wen, H. Nagamoto, and H. Takahashi, J. Appl. Electrochem. **35**, 865 (2005).
[6] G. A. Samara, Ferroelectrics **71**, 161 (1987).
[7] K. Deguchi, S. Azuma, Y. Kobayashi, S. Endo, and M. Tokunaga, Phys. Rev. B **69**, 024106 (2004).
[8] Y. Iwata, K. Deguchi, S. Mitani, I. Shibuya, Y. Onodera, and E. Nakamura, J. Phys. Soc. Jpn. **63**, 4044 (1994).
[9] M. I. McMahon, R. J. Nelmes, W. F. Kuhs, R. Dorwarth, R. O. Piltz, and Z. Tun, Nature (London) **348**, 317 (1990).
[10] J. M. Robertson and A. R. Ubbelohde, Proc. R. Soc. London A **170**, 222 (1939).
[11] N. Kojyo and Y. Onodera, J. Phys. Soc. Jpn. **57**, 4391 (1988).
[12] R. Blinc, J. Phys. Chem. Solids **13**, 204 (1960).
[13] S. Koval, J. Kohanoff, R. L. Migoni, and E. Tosatti, Phys. Rev. Lett. **89**, 187602 (2002).
[14] S. Koval, J. Kohanoff, J. Lasave, G. Colizzi, and R. L. Migoni, Phys. Rev. B **71**, 184102 (2005).
[15] V. Srinivasan and D. Sebastiani, J. Phys. Chem. C **115**, 12631 (2011).
[16] K. T. Wikfeldt and A. Michaelides, J. Chem. Phys. **140**, 041103 (2014).
[17] K. T. Wikfeldt, J. Phys. Conf. Ser. **571**, 012012 (2014).
[18] K. Deguchi, E. Okaue, and E. Nakamura, J. Phys. Soc. Jpn. **51**, 3569 (1982).
[19] G. A. Samara, Ferroelectrics **5**, 25 (1973).
[20] R. J. Nelmes and R. N. P. Choudhary, Sol. St. Comm. **26**, 823 (1978).
[21] Y. Shchur, Phys. Rev. B **74**, 054301 (2006).
[22] D. Semmingsen, W. D. Ellenson, B. C. Frazer, and G. Shirane, Phys. Rev. Lett. **38**, 1299 (1977).

[23] R. Blinc, B. Zeks, A. Levstik, C. Filipic, J. Slak, M. Burgar, I. Zupancic, L. A. Shuvalov, and A. I. Baranov, Phys. Rev. Lett. **43**, 231 (1979).

[24] S. Shin, A. Ishida, T. Yamakami, T. Fujimura, and M. Ishigame, Phys. Rev. B **35**, 4455 (1987).

[25] K. Imai and H. Ishida, J. Phys. Soc. Jpn. **56**, 347 (1987).

[26] P. J. Schuele and V. H. Schmidt, Phys. Rev. B **39**, 2549 (1989).

[27] S. Koval, J. Kohanoff, R. L. Migoni, and A. Bussmann-Holder, Comput. Mater. Sci. **22**, 87 (2001).

[28] Q. Zhang, F. Chen, N. Kioussis, S. G. Demos, and H. B. Radousky, Phys. Rev. B **65**, 024108 (2001).

[29] J. Lasave, S. Koval, N. S. Dalal, and R. L. Migoni, Phys. Rev. Lett. **98**, 267601 (2007).

[30] G. Colizzi, J. Kohanoff, J. Lasave, and R Migoni, Ferroelectrics **401**, 200 (2010).

[31] J. Lasave, S. Koval, R. L. Migoni, and N. S. Dalal, J. Chem. Phys. **135**, 084504 (2011).

[32] N. S. Dalal, J. A. Hebden, D. E. Kennedy, and C. A. McDowell, J. Chem. Phys. **66**, 4425 (1976).

[33] F. Zamponi, P. Rothhardt, J. Stingl, M. Woerner, and T. Elsaesser, Proc. Natl. Ac. Sc. **109**, 5207 (2012).

[34] M. I. McMahon, R. J. Nelmes, R. O. Piltz, and W. F. Kuhs, Europhys. Lett. **13**, 143 (1990).

[35] M. I. McMahon, R. J. Nelmes, R. O. Piltz, W. F. Kuhs, and N. G. Wright, Ferroelectrics **124**, 351 (1991).

[36] G. F. Reiter, J. Mayers, and P. Platzman, Phys. Rev. Lett. **89**, 135505 (2002).

[37] G. Reiter, A. Shukla, P. M. Platzman, and J. Mayers, New. J. Phys. **10**, 013016 (2008).

[38] S. Horiuchi, R. Kumai, and Y. Tokura, Angew. Chem. Int. Ed. **46**, 3497 (2007).

[39] S. Horiuchi, R. Kumai, and Y. Tokura, Chem. Commun. 2321 (2007).

[40] S. Horiuchi and Y. Tokura, Nat. Mater. **7**, 357 (2008).

[41] D. Braga, L. Maini, and F. Grepioni, Cryst. Eng. Comm. **3**, 27 (2001).

[42] S. Horiuchi, Y. Tokunaga, G. Giovannetti, S. Picozzi, H. Itoh, R. Shimano, R. Kumai, and Y. Tokura, Nature (London) **463**, 789 (2010).

[43] D. Di Sante, A. Stroppa, and S. Picozzi, Phys. Chem. Chem. Phys. **14**, 14673 (2012).

[44] K. Lee, B. Kolb, T. Thonhauser, D. Vanderbilt, and D. C. Langreth, Phys. Rev. B **86**, 104102 (2012).

[45] P. Giannozzi, S. Baroni, N. Bonini, M. Calandra, R. Car, C. Cavazzoni, D. Ceresoli, G. L. Chiarotti, M. Cococcioni, I. Dabo, A. Dal Corso, S. de Gironcoli, S. Fabris, G. Frates, R. Gebauer, U. Gerstmann, C. Gougoussis, A. Kokalj, M. Lazzeri, L. Martin-Samos, N. Marzari, F. Mauri, R. Mazzarello, S. Paolini, A. Pasquarello, L. Paulatto, C. Sbraccia, S. Scandolo, G. Sclauzero, A. P. Seitsonen, A. Smogunov, P. Umari, and R. M. Wentzcovitch, J. Phys. Condens. Matter **21**, 395502 (2009).

[46] G. Kresse and J. Furthmuller, Comput. Mater. Sci. **6**, 15 (1996).

[47] G. Kresse and J. Furthmuller, Phys. Rev. B **54**, 11169 (1996).

[48] N. Troullier and J. L. Martins, Phys. Rev. B **43**, 1993 (1991).

[49] G. Kresse and D. Joubert, Phys. Rev. B **59**, 1758 (1999).

[50] H. J. Monkhorst and J. D. Pack, Phys. Rev. B **13**, 5188 (1976).

[51] J. Lasave, J. Kohanoff, R. L. Migoni, and S. Koval, Physica B **404**, 2736 (2009).

[52] S. Koval, J. Lasave, J. Kohanoff, and R. Migoni, Ferroelectrics **401**, 103 (2010).

[53] R. D. King-Smith and D. Vanderbilt, Phys. Rev. B **47**, 1651(R) (1993).

[54] R. Resta, Rev. Mod. Phys. **66**, 899 (1994).

[55] N. A. Spaldin, J. Sol. St. Chem. **195**, 2 (2012).

[56] F. Bernardini, V. Fiorentini, and David Vanderbilt, Phys. Rev. B **63**, 193201 (2001).

[57] J. B. Neaton, C. Ederer, U. V. Waghmare, N. A. Spaldin, and K. M. Rabe, Phys. Rev. B **71**, 014113 (2005).

[58] A. Stroppa, D. Di Sante, S. Horiuchi, Y. Tokura, D. Vanderbilt, and S. Picozzi, Phys. Rev. B **84**, 014101 (2011).

[59] M. Dion, H. Rydberg, E. Schroder, D. C. Langreth, and B. I. Lundqvist, Phys. Rev. Lett. **92**, 246401 (2004).

[60] J. Klimeš, D. R. Bowler, and A. Michaelides, Phys. Rev. B **83**, 195131 (2011).

[61] G. Román-Pérez and J. M. Soler, Phys. Rev. Lett. **103**, 096102 (2009).

[62] K. Lee, E. D. Murray, L. Kong, B. I. Lundqvist, and D. C. Langreth, Phys. Rev. B **82**, 081101 (2010).

[63] J. Klimeš, D. R. Bowler, and A. Michaelides, J. Phys. Condens. Matter **22**, 022201 (2010).

[64] S. Grimme, J. Comp. Chem. **27**, 1787 (2006).

[65] A. Tkatchenko and M. Scheffler, Phys. Rev. Lett. **102**, 073005 (2009).

[66] J. P. Perdew, K. Burke, and M. Ernzerhof, Phys. Rev. Lett. **77**, 3865 (1996).

[67] C. Adamo and V. Barone, J. Chem. Phys. **110**, 6158 (1999).

[68] C. Chakravarty, Int. Rev. Phys. Chem. **16**, 421 (1997).

[69] F. Torresi, J. Lasave, and S. Koval (unpublished).

[70] E. Matsushita and T. Matsubara, Prog. Theor. Phys. **67**, 1 (1982).

[71] X. Li, B. Walker, and A. Michaelides, Proc. Natl. Acad. Sci. USA **108**, 6369 (2011).

[72] G. A. Samara and D. Semmingsen, J. Chem. Phys. **71**, 1401 (1979).

[73] A. R. Grimm, G. B. Bacskay, and A. D. J. Haymet, Mol. Phys. **86**, 369 (1995).

[74] S. Baroni, S. de Gironcoli, A. dal Corso, and P. Gianozzi, Rev. Mod. Phys. **73**, 515 (2001).

[75] I. Scivetti, N. Gidopoulos, and J. Kohanoff, Phys. Rev. B **78**, 224108 (2008).

[76] R. H. McKenzie, C. Bekker, B. Athokpam, and S. G. Ramesh, J. Chem. Phys. **140**, 174508 (2014).

[77] B. C. Frazer, D. Semmingsen, W. D. Ellenson, and G. Shirane, Phys. Rev. B **20**, 2745 (1979).

[78] K. Itoh, T. Hagiwara, and E. Nakamura, J. Phys. Soc. Jpn. **52**, 2626 (1983).

[79] R. J. Nelmes, M. I. McMahon R. O. Piltz, and N. G. Wright, Ferroelectrics **124**, 355 (1991).

[80] J. A. Morrone, L. Lin, and R. Car, J. Chem. Phys. **130**, 204511 (2009).

[81] H. Matsunaga, K. Itoh, and E. Nakamura, J. Phys. Soc. Jpn. **48**, 2011 (1980).